THE JOURNAL OF PHYSICAL CHEMISTRY LETTERS
A JOURNAL OF THE AMERICAN CHEMICAL SOCIETY

pubs.acs.org/JPCL

Letter

Electron-Volt Fluctuation of Defect Levels in Metal Halide Perovskites on a 100 ps Time Scale

Bipeng Wang, Weibin Chu, Yifan Wu, David Casanova, Wissam A. Saidi, and Oleg V. Prezhdo*

Cite This: *J. Phys. Chem. Lett.* 2022, 13, 5946−5952

Read Online

ACCESS | Metrics & More | Article Recommendations | Supporting Information

ABSTRACT: Metal halide perovskites (MHPs) have gained considerable attention due to their excellent optoelectronic performance, which is often attributed to unusual defect properties. We demonstrate that midgap defect levels can exhibit very large and slow energy fluctuations associated with anharmonic acoustic motions. Therefore, care should be taken classifying MHP defects as deep or shallow, since shallow defects may become deep and vice versa. As a consequence, charges from deep levels can escape into bands, and light absorption can be extended to longer wavelengths, improving material performance. The phenomenon, demonstrated with iodine vacancy in $CH_3NH_3PbI_3$ using a machine learning force field, can be expected for a variety of defects and dopants in many MHPs and other soft inorganic semiconductors. Since large-scale anharmonic motions can be precursors to chemical decomposition, a known problem with MHPs, we propose that materials that are stiffer than MHPs but softer than traditional inorganic semiconductors, such as Si and TiO_2, may simultaneously exhibit excellent performance and stability.

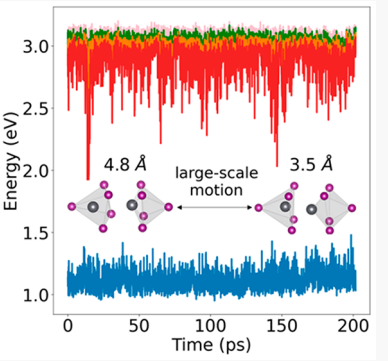

Metal halide perovskites (MHPs) are attractive both scientifically and industrially because of their low manufacturing cost and excellent electronic and optical properties, including strong light absorption, tunable band gap, and long charge carrier diffusion.[1−5] Solar cells based on MHPs convert solar energy to electricity with high power conversion efficiency that has grown rapidly from 3.8% to 25.7%.[6−8] MHPs are much softer than Si, GaAs, TiO_2, and other inorganic semiconductors that form the basis for efficient solar cells. Combining the properties of inorganic, organic, and even liquid[9] matter, MHPs are able to conduct charges over distances longer than 1 μm, screen electron−hole interactions, and decouple free charges from defect states, producing carrier lifetimes exceeding 1 μs.[10] The complex composition and geometric structure of MHPs and their softness can give rise to significant thermal fluctuations over a variety of time scales. It has been demonstrated that defect energy levels fluctuate much more in MHPs than traditional inorganic semiconductors, such as GaAs.[11] Energy level fluctuations play important roles in charge carrier trapping and recombination dynamics.[12−16] Proper modeling of thermal fluctuations in MHPs is challenging by ab initio density functional theory (DFT), which is limited to systems composed of hundreds of atoms and picosecond time scales. While scientists have already found many important and unusual properties with ab initio calculations, rationalizing high defect tolerance[15−20] and large carrier lifetimes,[21−24] longer molecular dynamics (MD) simulations with larger systems can uncover further unusual structural and electronic features of MHPs.

Machine learning (ML) force fields (FFs) trained based on ab initio DFT data allow one to obtain ab initio quality results at a fraction of the computational cost. Structural motifs of condensed matter systems make it intuitive to generate global and local descriptors and obtain physically motivated FFs. Thus, Tkatchenko and co-workers developed a Bravais-inspired gradient-domain ML model employing Bravais symmetry groups and global descriptors based on the Coulomb matrix.[25] Csanyi and co-workers used the smooth overlap of atomic positions to develop a Gaussian potential ML model.[26] Behler, Goedecker, and co-workers developed fourth-generation high-dimensional neural network potentials with local atom-centered symmetry functions.[27] These applications of ML in modeling atomic FFs are successful in predicting the structural dynamics and total energy of molecules and bulk systems.[28−31] A description of excited electronic states with ML is more challenging because they are more complex functions of system geometries than ground states. Particularly relevant for solar energy applications are ML efforts to extend the range of nonadiabatic MD simulations, which allow one to model charge separation, trapping, and recombination processes that govern solar cell efficiencies.[12−16,32−38]

In this Letter, we demonstrate that defect levels in MHPs can fluctuate very significantly on slow time scales associated

Received: May 13, 2022
Accepted: June 17, 2022
Published: June 22, 2022

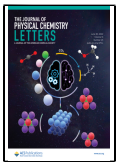

https://doi.org/10.1021/acs.jpclett.2c01452
J. Phys. Chem. Lett. 2022, 13, 5946−5952

with anharmonic acoustic motions of the soft inorganic lattice. Focusing on an iodine vacancy in $MAPbI_3$ ($MA = CH_3NH_3$), a common defect in the classic MHP, we develop an ML FF that allows us to generate nanosecond MD trajectories and to analyze them by ab initio DFT. At 0 K with the optimized structure, the vacancy creates no midgap levels. However, at ambient temperature, up to three deep levels can be created spanning more than half of the fundamental band gap. The defect level properties correlate with the distance between the two Pb atoms across the vacancy. Changes in the Pb−Pb distance require large-scale concerted rearrangements of the $MAPbI_3$ inorganic lattice, rationalizing the slow time scale. We hypothesize that similar fluctuations are possible with many defects and dopants in other MHPs and related soft inorganic materials and that such defect level fluctuations are essential for excellent MHP performance.

The ab initio DFT calculations were performed with the Vienna Ab initio Simulation Package[39] (VASP). The Perdew−Burke−Ernzerhof (PBE) density functional[40] and projected augmented pseudopotentials[41] were used. The cutoff energy of the plane wave basis was set to 450 eV. The convergence for the energy and the forces were 10^{-7} eV and 10^{-3} eV/Å, respectively. A large simulation cell consisting of $4 \times 2 \times 2$ unit cells and 383 atoms was employed to model $MAPbI_3$. An iodine atom was removed from the pristine system to create an iodine vacancy in $MAPbI_3$. The structures were visualized with the VESTA software package.[42] The ML FF was developed as described in detail in refs 43−50 and summarized in the Supporting Information (SI).

Figure 1a shows the optimized ab initio geometry of $MAPbI_3$ containing an iodine vacancy, with the vacancy region

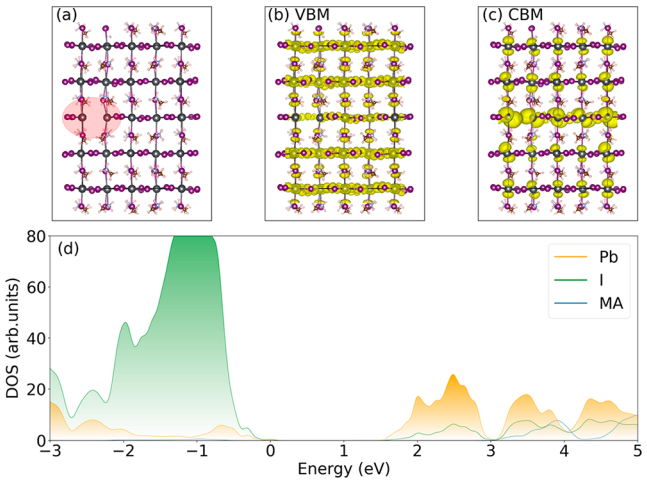

Figure 1. (a) Optimized structure of $MAPbI_3$ with the iodine vacancy between two lead atoms shaded in red. (b, c) Charge density of the VBM and CBM of the defective system. (d) Corresponding projected DOS with zero energy set to the VBM.

shaded in pink. Figure 1b,c presents the charge densities of the valence band maximum (VBM) and conduction band minimum (CBM). The distance between the two Pb atoms across the vacancy is large, 6.05 Å, and is similar to the distance between Pb atoms in the pristine regions. The VBM and CBM are delocalized, with the vacancy region differing little from the pristine regions. The CBM shows an area of increased pancakelike charge density.[51,52] The VBM is mainly supported by iodines, while the CBM is primarily localized on Pb atoms. The VBM−CBM energy gap is 1.62 eV in the optimized structure, and no midgap states are created by the iodine vacancy defect.

Having trained the ML FF based on the ab initio DFT input, we heated the system to 300 K, obtained a 3 ns long microcanonical trajectory, and analyzed a randomly selected 200 ps part with ab initio DFT. We observe very significant fluctuations in the electronic energy levels occurring on a 50−100 ps time scale (Figure 2a). The fluctuations are on the order of 1 eV and reduce the band gap of the defective $MAPbI_3$ from 1.62 eV in the optimized geometry to as little as 0.5 eV. This observation is very significant. On one hand, deep defects can accelerate charge carrier recombination. On the other hand, they can extend light harvesting far into the infrared (IR) region. Moreover, the large fluctuations in the defect levels can allow charge carriers with energies of only 0.5 eV relative to the ground state to escape into valence and conduction bands separated by over 1.5 eV. Large fluctuations in the defect level energies were observed previously with ab initio MD[11−16] on shorter, 10 ps time scales.

In order to test that the observation is not an artifact of the ML FF, we analyzed the FF quality. In addition to the standard measures taken during the ML FF training,[43−50] we compared the ab initio and ML potential energies in the region with the deepest energy level fluctuation between 10 and 17 ps (Figure 2a). The ab initio and ML potential energies follow each other, as shown in Figure S1 of the Supporting Information. The root mean squared (RMS) error of the ML energy relative to the corresponding ab initio values, i.e., the RMS energy difference, is only 0.33 eV per system containing 383 atoms, or 0.86 meV/atom.

An important insight into the origin of the large and slow fluctuation of the defect energy levels is provided by the distance between the Pb atoms surrounding the vacancy. These are the two Pb atoms that would have coordinated the iodine atom if it had been present in the system. The equilibrium Pb−Pb distance is equal to 6.05 Å in the optimized structure. The Pb−Pb distance across the vacancy is much shorter at ambient conditions. It fluctuates between 3.49 and 4.81 Å along the 200 ps trajectory (Figure 2c). The distance correlates very well with the defect level energy. This can be seen by comparing the 200 ps data in Figure 2a,c and even better from the 10 to 17 ps data in Figure 2b,d. When the Pb−Pb distance is short, the trap levels become deep. When the distance approaches its minimal value of 3.5 Å, up to three deep trap levels appear inside the band gap of $MAPbI_3$ with the iodine vacancy. As the Pb atoms move away from each other, the number of deep traps decreases to 2, 1, or 0.

Four representative defect configurations and the corresponding densities of states (DOS) are shown in Figure 3. Figure 4 and Figures S2−S5 present the corresponding charge densities. When the distance between the Pb atoms is large, 4.81 Å (Figure 3a), no trap states are observed. The transient disappearance of midgap levels is beneficial for charge transport, since trapped charges can escape into the bands at this instance. The VBM and CBM charge densities are partially localized (Figure S2) compared to the VBM and CBM for the optimized structure (Figure 1b,c). This moderate localization of charge carriers inside bands arises from large anharmonicity of MHP motions[53] and rationalizes[53−55] the observed[56] and unusual increase of the charge carrier lifetimes with increasing temperature. The electron−hole overlap decreases with temperature, and the electron−phonon coupling becomes

https://doi.org/10.1021/acs.jpclett.2c01452
J. Phys. Chem. Lett. 2022, 13, 5946−5952

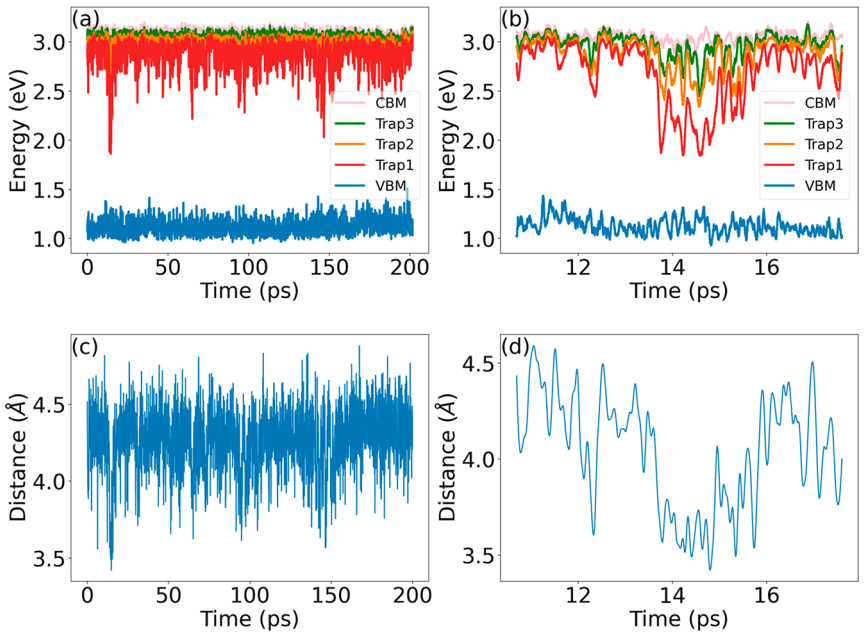

Figure 2. (a) Energy levels of the VBM, 3 traps, and CBM in the defective $MAPbI_3$. The data points are selected every 64 fs. (b) Zoomed-in view on the energy levels of the first deep-trap region between 10 and 17 ps. A comparison of the ab initio and ML potential energies is provided in Figure S1. (c) Fluctuation of the distance between the two Pb atoms around the iodine vacancy over 200 ps. (d) Fluctuation of the distance between the two Pb atoms from 10 to 17 ps. The 1 eV drop in the defect energy level is associated with the 1 Å shortening of the Pb−Pb distance. This phenomenon occurs about every 50 ps.

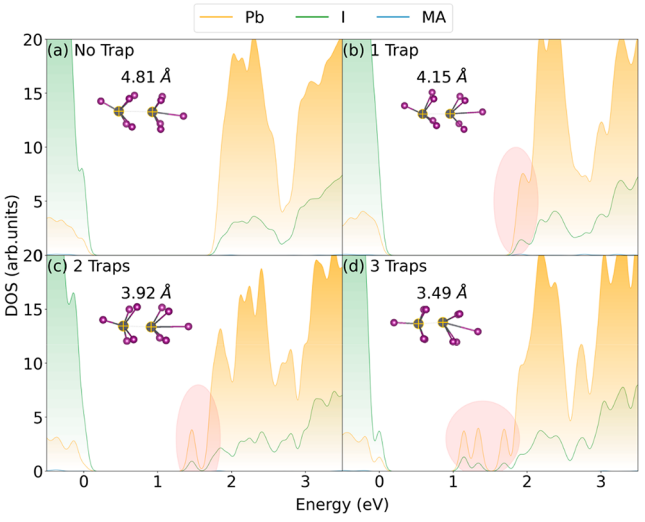

Figure 3. (a−d) Projected DOS of the defective $MAPbI_3$ at different MD times. As the Pb−Pb distance fluctuates from 4.81 to 3.49 Å, the number of midgap trap states fluctuates from zero to three. The trap states are shaded by pink. The corresponding charge densities are shown in Figure 4 and Figures S2−S5.

weaker, even though the atomic velocity grows.[55,57] Note that although the carrier lifetime increases with temperature, heating can accelerate MHP degradation.[58−60]

Anharmonicity plays many important roles in MHPs. In addition to causing moderate carrier localization and growth of lifetime with temperature, anharmonicity gives rise to rapid elastic charge−phonon scattering, which shortens coherence time between excited and ground states and extends charge carrier lifetimes.[53,61,62] Strongly anharmonic rotations of the organic MA cations contribute significantly to charge screening, exciton dissociation, and polaron formation, also extending carrier lifetimes.[62−64] Anharmonicity allows interactions between different parts of perovskites, leading to the formation of new chemical species in the excited state that change trap state energies[13,60] and lead to photochemical decomposition.[58−60] Other types of MHPs exhibit weaker anharmonicity and, as a consequence, decreased carrier lifetimes at elevated temperatures.[65,66]

When the Pb−Pb distance is shortened to 4.15 Å (Figure 3b), an electron trap appears close to the CBM, localizing notably near the vacancy, VBM+1 in Figure S3. A second trap appears when the Pb−Pb distance decreases below 4 Å (Figure 3c). Both VBM+1 and VBM+2 charge densities become localized near the vacancy (Figure S4). Three trap states are observed for the shortest distances around 3.5 Å (Figure 3d and Figure S5).

Figure 4 provides a closer view of the charge densities of the three trap states corresponding to the structure in Figure 3d. The levels originate primarily from p-orbitals of the two surrounding Pb atoms, shown in red in Figure 4. The contributions of the p-orbitals to these levels, obtained from VASP PROCAR files as *spd*- and site-projected wave function character, are summarized in Table 1. Trap 1 is the deepest trap whose energy is most strongly affected by the Pb−Pb distance. Correspondingly, its charge density is localized on both Pb atoms (Figure 4a) and has the largest contribution from the p_x-orbitals that point along the Pb−Pb direction (Table 1). The second deepest trap state, i.e., Trap 2, has a different orientation and is localized on the right Pb atom, with the largest contribution stemming from the p_y-orbital. The third and shallowest state (Trap 3) is also localized on the right Pb atom. It is perpendicular to the other two traps, originating largely from the p_z-orbital (Table 1).

Further insights into the origin of the defect level fluctuation are provided by Fourier transforms (FTs) of the VBM, CBM, and trap level energies, computed based on the trajectory data

https://doi.org/10.1021/acs.jpclett.2c01452
J. Phys. Chem. Lett. 2022, 13, 5946−5952

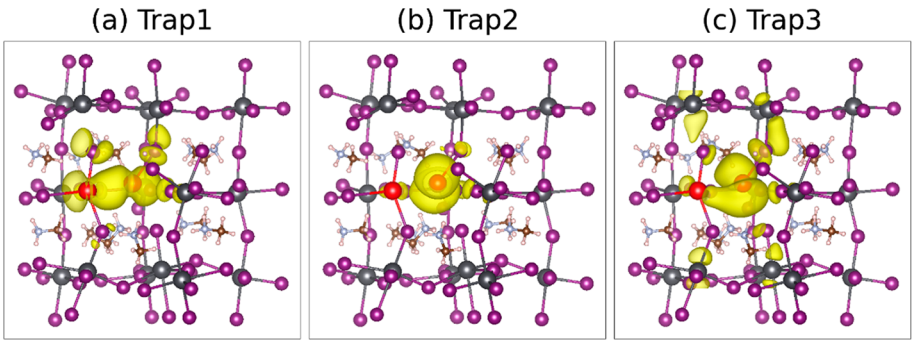

Figure 4. (a–c) Charge densities of the three midgap trap state in the defective $MAPbI_3$ corresponding to Figure 3d. The Pb atoms next to the vacancy are shown in red. The trap states are formed by p-orbitals of the Pb atoms (Table 1).

Table 1. Contribution of the p-Orbitals of the Two Pb Atoms to the Three Traps Shown in Figure 4

		p_x	p_y	p_z
Trap1	Pb (right)	0.141	0.078	0.000
	Pb (left)	0.117	0.053	0.000
Trap2	Pb (right)	0.103	0.238	0.092
	Pb (left)	0.000	0.000	0.004
Trap3	Pb (right)	0.064	0.015	0.212
	Pb (left)	0.020	0.000	0.003

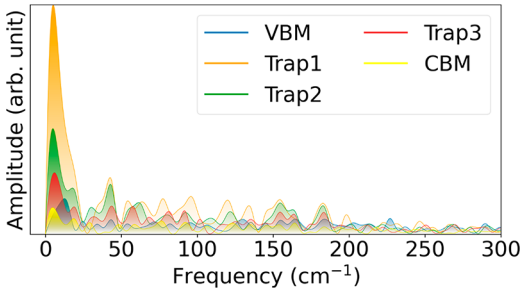

Figure 5. Fourier transforms of the energies of the key states in the defective $MAPbI_3$ for the time from 10 to 17 ps (Figure 2). The same frequencies contribute to the oscillations of the VBM, CBM, and trap states; however, deeper traps oscillate with larger amplitude, as reflected in the stronger low-frequency FT signals.

between 10 and 17 ps (Figure 5). These influence spectra, or spectral densities, are heavily dominated by very low frequencies. The importance of low-frequency motions for the electron-vibrational coupling responsible for nonradiative relaxation has been established in other nanoscale and condensed matter systems;[61,67−72] however, the frequencies are particularly low in MHPs, since MHPs are soft.[15,16] Such low-frequency motions arise from slow acoustic modes that involve large concerted displacements and tilting of MHP octahedra, bringing the two Pb atoms across the vacancy closer and farther away from each other. While the high-frequency signals are comparable for the VBM, CBM, and trap states, the low-frequency signals are much stronger for the trap states. Further, the deeper the trap, the stronger the low-frequency signal. The amplitude of the FT signal is determined by the energy level fluctuation. The RMS fluctuations of the VBM and CBM levels are 0.08 and 0.05 eV, respectively, calculated using the 10−17 ps part of the MD trajectory. The corresponding fluctuations of Trap 3, Trap 2, and Trap 1 are notably larger: 0.31, 0.17, and 0.11 eV, respectively. The high-frequency signals are weaker by an order of magnitude compared to the low-frequency signals. This is because the trap state energies are influenced primarily by the Pb−Pb distance, whose variation requires acoustic-type large-scale motions. The VBM and CBM levels are not particularly sensitive to fast optical-type atomic vibrations either, most likely because the phase of such vibrations changes rapidly across the system, and contributions from different atoms cancel. Larger simulation cells can generate even lower-frequency motions that may lead to other changes in the MHP electronic properties.

In summary, we have demonstrated a large, up to 1 eV fluctuation of defect energy levels in $MAPbI_3$, occurring on a 50−100 ps time scale. The phenomenon is seen in MHPs but not other more traditional inorganic semiconductors, such as Si or GaAs, because MHPs are much softer and anharmonic, exhibiting large-scale atom displacements. The defect level fluctuation is important for applications. *First*, the fluctuation indicates that defects considered shallow based on static calculations performed with optimized structures can be deep at ambient conditions. Typically, deep defects are considered detrimental to semiconductor performance because they create efficient charge recombination centers. However, the argument does not necessarily apply to MHPs, since the levels in the current example are deep only for a short period of time. *Second*, defects considered deep based on static calculations can fluctuate toward band edges, allowing charges to escape into bands, reducing trap-mediated charge recombination. While MHP defects can be classified as shallow or deep based on the defect state energies at equilibrium geometries, it is important to extend the standard classification to characterize the defect energy fluctuation. *Third*, by fluctuating between shallow and deep states, defects in MHPs create an opportunity for light absorption across a broader energy range, extending to wavelengths much longer than the wavelength corresponding to the fundamental band gap. The energy range of absorbed light is often extended in traditional inorganic semiconductors, such as TiO_2, by doping.[73,74] The dopant concentration has to be high in order to create dopant energy bands and achieve good charge transport in such cases. The traditional strategy can be reconsidered if energy levels of dopants in MHPs fluctuate significantly, allowing harvested charges to escape into the intrinsic bands. Additional studies are required to evaluate absorbance of deep defect levels and to select dopants that maximize the absorption while still allowing charges to escape from deep levels by the defect level fluctuation mechanism. The competition between defect-mediated charge recombination and charge escape into bands can be studied by nonadiabatic MD simulation.[24,35,75−81]

https://doi.org/10.1021/acs.jpclett.2c01452
J. Phys. Chem. Lett. 2022, 13, 5946−5952

The demonstration of the large-scale and slow fluctuation of the defect energy levels is possible as a result of the development of ab initio quality ML FFs. A direct ab initio evaluation of the phenomenon is harder due to the computational expense. In the case of the iodine vacancy, the defect energy level fluctuation has been rationalized atomistically by considering the local defect structure. The level with the largest fluctuation is supported by the p-orbitals of the Pb atoms that can form a bond across the vacancy. The bond formation requires a concerted, large-scale, and slow displacement of the $MAPbI_3$ structure involving deformation and tilting of the PbI_6 octahedra. Compared to the traditional inorganic semiconductors, such as Si, GaAs, TiO_2, etc., such highly anharmonic acoustic motions are possible in MHPs because they are much softer. Similar beneficial defect properties can be expected in other classes of soft materials that are able to maintain good charge transport. Further, poor chemical stability constitutes a major drawback of MPHs. Poor stability can be associated with large-scale atomic motions discussed here, which may act as precursors to chemical decomposition. If this is the case, then one can attempt to search for materials that are somewhat stiffer than MHPs. Such materials could be more stable and still maintain the desirable defect properties.

■ ASSOCIATED CONTENT

Supporting Information

The Supporting Information is available free of charge at https://pubs.acs.org/doi/10.1021/acs.jpclett.2c01452.

Comparison between ab initio and ML potential energies and representative charge densities of the VBM, CBM, and trap states; and details of the ML FF training (PDF)

■ AUTHOR INFORMATION

Corresponding Author

Oleg V. Prezhdo − *Department of Chemical Engineering, University of Southern California, Los Angeles, California 90089, United States; Department of Chemistry, University of Southern California, Los Angeles, California 90089, United States;* orcid.org/0000-0002-5140-7500; Email: prezhdo@usc.edu

Authors

Bipeng Wang − *Department of Chemical Engineering, University of Southern California, Los Angeles, California 90089, United States;* orcid.org/0000-0003-0924-5867

Weibin Chu − *Department of Chemistry, University of Southern California, Los Angeles, California 90089, United States;* orcid.org/0000-0001-5951-0337

Yifan Wu − *Department of Chemistry, University of Southern California, Los Angeles, California 90089, United States*

David Casanova − *Donostia International Physics Center (DIPC), Donostia 20018 Euskadi, Spain; Basque Foundation for Science, IKERBASQUE, Bilbao 48009 Euskadi, Spain;* orcid.org/0000-0002-8893-7089

Wissam A. Saidi − *Department of Mechanical Engineering & Materials Science, University of Pittsburgh, Pittsburgh, Pennsylvania 15261, United States;* orcid.org/0000-0001-6714-4832

Complete contact information is available at: https://pubs.acs.org/10.1021/acs.jpclett.2c01452

Notes

The authors declare no competing financial interest.

■ ACKNOWLEDGMENTS

The research was supported by the US National Science Foundation, grant CHE-2154367. W.A.S. was supported by the US National Science Foundation, Award No. CSSI-2003808. D.C. thanks the support from Ministerio de Ciencia e Innovación (MICINN) of Spain (project PID2019-109555GB-I00) and the Eusko Jaurlaritza/Basque Government (projects PIBA19-0004 and 2019-CIEN-000092-01). We are grateful for computing time provided in by the University of Southern California High Performance Computing Center and the Center for Research Computing at the University of Pittsburgh.

■ REFERENCES

(1) Yin, W. J.; Shi, T. T.; Yan, Y. F. Unique Properties of Halide Perovskites as Possible Origins of the Superior Solar Cell Performance. *Adv. Mater.* **2014**, *26*, 4653−4658.

(2) Hao, F.; Stoumpos, C. C.; Chang, R. P. H.; Kanatzidis, M. G. Anomalous Band Gap Behavior in Mixed Sn and Pb Perovskites Enables Broadening of Absorption Spectrum in Solar Cells. *J. Am. Chem. Soc.* **2014**, *136*, 8094−8099.

(3) Stranks, S. D.; Eperon, G. E.; Grancini, G.; Menelaou, C.; Alcocer, M. J. P.; Leijtens, T.; Herz, L. M.; Petrozza, A.; Snaith, H. J. Electron-Hole Diffusion Lengths Exceeding 1 Micrometer in an Organometal Trihalide Perovskite Absorber. *Science* **2013**, *342*, 341−344.

(4) Xing, G. C.; Mathews, N.; Sun, S. Y.; Lim, S. S.; Lam, Y. M.; Gratzel, M.; Mhaisalkar, S.; Sum, T. C. Long-Range Balanced Electron- and Hole-Transport Lengths in Organic-Inorganic CH3NH3PbI3. *Science* **2013**, *342*, 344−347.

(5) Grancini, G.; Marras, S.; Prato, M.; Giannini, C.; Quarti, C.; De Angelis, F.; De Bastiani, M.; Eperon, G. E.; Snaith, H. J.; Manna, L.; et al. The Impact of the Crystallization Processes on the Structural and Optical Properties of Hybrid Perovskite Films for Photovoltaics. *J. Phys. Chem. Lett.* **2014**, *5*, 3836−3842.

(6) Kojima, A.; Teshima, K.; Shirai, Y.; Miyasaka, T. Organometal Halide Perovskites as Visible-Light Sensitizers for Photovoltaic Cells. *J. Am. Chem. Soc.* **2009**, *131*, 6050−6051.

(7) Lee, M. M.; Teuscher, J.; Miyasaka, T.; Murakami, T. N.; Snaith, H. J. Efficient Hybrid Solar Cells Based on Meso-Superstructured Organometal Halide Perovskites. *Science* **2012**, *338*, 643−647.

(8) Kim, M.; Jeong, J.; Lu, H. Z.; Lee, T. K.; Eickemeyer, F. T.; Liu, Y. H.; Choi, I. W.; Choi, S. J.; Jo, Y.; Kim, H. B.; et al. Conformal Quantum Dot-Sno2 Layers as Electron Transporters for Efficient Perovskite Solar Cells. *Science* **2022**, *375*, 302−306.

(9) Seiler, H.; Palato, S.; Sonnichsen, C.; Baker, H.; Socie, E.; Strandell, D. P.; Kambhampati, P. Two-Dimensional Electronic Spectroscopy Reveals Liquid-Like Lineshape Dynamics in CsPbI3 Perovskite Nanocrystals. *Nat. Commun.* **2019**, *10*, 4962.

(10) Bou, A.; Abolins, H.; Ashoka, A.; Cruanyes, H.; Guerrero, A.; Deschler, F.; Bisquert, J. Extracting in Situ Charge Carrier Diffusion Parameters in Perovskite Solar Cells with Light Modulated Techniques. *ACS Energy Lett.* **2021**, *6*, 2248−2255.

(11) Cohen, A. V.; Egger, D. A.; Rappe, A. M.; Kronik, L. Breakdown of the Static Picture of Defect Energetics in Halide Perovskites: The Case of the Br Vacancy in CsPbBr3. *J. Phys. Chem. Lett.* **2019**, *10*, 4490−4498.

(12) Li, W.; Liu, J.; Bai, F. Q.; Zhang, H. X.; Prezhdo, O. V. Hole Trapping by Iodine Interstitial Defects Decreases Free Carrier Losses in Perovskite Solar Cells: A Time-Domain Ab Initio Study. *ACS Energy Lett.* **2017**, *2*, 1270−1278.

(13) Li, W.; Sun, Y. Y.; Li, L. Q.; Zhou, Z. H.; Tang, J. F.; Prezhdo, O. V. Control of Charge Recombination in Perovskites by Oxidation State of Halide Vacancy. *J. Am. Chem. Soc.* **2018**, *140*, 15753−15763.

(14) Li, W.; Long, R.; Tang, J. F.; Prezhdo, O. V. Influence of Defects on Excited-State Dynamics in Lead Halide Perovskites: Time-Domain Ab Initio Studies. *J. Phys. Chem. Lett.* **2019**, *10*, 3788−3804.
(15) Chu, W. B.; Saidi, W. A.; Zhao, J.; Prezhdo, O. V. Soft Lattice and Defect Covalency Rationalize Tolerance of Beta-CsPbI3 Perovskite Solar Cells to Native Defects. *Angew. Chem., Int. Ed.* **2020**, *59*, 6435−6441.
(16) Chu, W. B.; Zheng, Q. J.; Prezhdo, O. V.; Zhao, J.; Saidi, W. A. Low-Frequency Lattice Phonons in Halide Perovskites Explain High Defect Tolerance toward Electron-Hole Recombination. *Sci. Adv.* **2020**, *6*, No. eaaw7453.
(17) Yin, W. J.; Shi, T. T.; Yan, Y. F. Unusual Defect Physics in CH3NH3PbI3 Perovskite Solar Cell Absorber. *Appl. Phys. Lett.* **2014**, *104*, 063903.
(18) Yin, W. J.; Shi, T. T.; Yan, Y. F. Superior Photovoltaic Properties of Lead Halide Perovskites: Insights from First-Principles Theory. *J. Phys. Chem. C* **2015**, *119*, 5253−5264.
(19) Huang, H.; Bodnarchuk, M. I.; Kershaw, S. V.; Kovalenko, M. V.; Rogach, A. L. Lead Halide Perovskite Nanocrystals in the Research Spotlight: Stability and Defect Tolerance. *ACS Energy Lett.* **2017**, *2*, 2071−2083.
(20) Kang, J.; Wang, L. W. High Defect Tolerance in Lead Halide Perovskite CsPbBr3. *J. Phys. Chem. Lett.* **2017**, *8*, 489−493.
(21) Frost, J. M.; Butler, K. T.; Brivio, F.; Hendon, C. H.; van Schilfgaarde, M.; Walsh, A. Atomistic Origins of High-Performance in Hybrid Halide Perovskite Solar Cells. *Nano Lett.* **2014**, *14*, 2584−2590.
(22) Amat, A.; Mosconi, E.; Ronca, E.; Quarti, C.; Umari, P.; Nazeeruddin, M. K.; Gratzel, M.; De Angelis, F. Cation-Induced Band-Gap Tuning in Organohalide Perovskites: Interplay of Spin-Orbit Coupling and Octahedra Tilting. *Nano Lett.* **2014**, *14*, 3608−3616.
(23) Nie, W. Y.; Tsai, H. H.; Asadpour, R.; Blancon, J. C.; Neukirch, A. J.; Gupta, G.; Crochet, J. J.; Chhowalla, M.; Tretiak, S.; Alam, M. A.; et al. High-Efficiency Solution-Processed Perovskite Solar Cells with Millimeter-Scale Grains. *Science* **2015**, *347*, 522−525.
(24) Li, W.; She, Y. L.; Vasenko, A. S.; Prezhdo, O. V. Ab Initio Nonadiabatic Molecular Dynamics of Charge Carriers in Metal Halide Perovskites. *Nanoscale* **2021**, *13*, 10239−10265.
(25) Chmiela, S.; Sauceda, H. E.; Poltavsky, I.; Muller, K. R.; Tkatchenko, A. Sgdml: Constructing Accurate and Data Efficient Molecular Force Fields Using Machine Learning. *Comput. Phys. Commun.* **2019**, *240*, 38−45.
(26) Bartok, A. P.; Kondor, R.; Csanyi, G. On Representing Chemical Environments. *Phys. Rev. B* **2013**, *87*, 16.
(27) Ko, T. W.; Finkler, J. A.; Goedecker, S.; Behler, J. A Fourth-Generation High-Dimensional Neural Network Potential with Accurate Electrostatics Including Non-Local Charge Transfer. *Nat. Commun.* **2021**, *12*, 11.
(28) Butler, K. T.; Davies, D. W.; Cartwright, H.; Isayev, O.; Walsh, A. Machine Learning for Molecular and Materials Science. *Nature* **2018**, *559*, 547−555.
(29) Cheng, B. Q.; Mazzola, G.; Pickard, C. J.; Ceriotti, M. Evidence for Supercritical Behaviour of High-Pressure Liquid Hydrogen. *Nature* **2020**, *585*, 217−220.
(30) Deringer, V. L.; Bernstein, N.; Csanyi, G.; Ben Mahmoud, C.; Ceriotti, M.; Wilson, M.; Drabold, D. A.; Elliott, S. R. Origins of Structural and Electronic Transitions in Disordered Silicon. *Nature* **2021**, *589*, 59−64.
(31) Poltavsky, I.; Tkatchenko, A. Machine Learning Force Fields: Recent Advances and Remaining Challenges. *J. Phys. Chem. Lett.* **2021**, *12*, 6551−6564.
(32) Hammes-Schiffer, S.; Soudackov, A. V. Proton-Coupled Electron Transfer in Solution, Proteins, and Electrochemistry. *J. Phys. Chem. B* **2008**, *112*, 14108−14123.
(33) Zimmerman, P. M.; Bell, F.; Casanova, D.; Head-Gordon, M. Mechanism for Singlet Fission in Pentacene and Tetracene: From Single Exciton to Two Triplets. *J. Am. Chem. Soc.* **2011**, *133*, 19944−19952.
(34) Huang, J. Q.; Zhao, X. Y.; Huang, X. K.; Liang, W. Z. Understanding the Mechanism of Plasmon-Driven Water Splitting: Hot Electron Injection and a near Field Enhancement Effect. *Phys. Chem. Chem. Phys.* **2021**, *23*, 25629−25636.
(35) Giannini, S.; Blumberger, J. Charge Transport in Organic Semiconductors: The Perspective from Nonadiabatic Molecular Dynamics. *Acc. Chem. Res.* **2022**, *55*, 819−830.
(36) Zhou, Z. B.; Ju, M. G.; Wang, J. L. Rational Unraveling of Alkali Metal Concentration-Dependent Photovoltaic Performance of Halide Perovskites: Octahedron Distortion Vs Surface Reconstruction. *J. Phys. Chem. Lett.* **2022**, *13*, 362−370.
(37) Shi, R.; Vasenko, A. S.; Long, R.; Prezhdo, O. V. Edge Influence on Charge Carrier Localization and Lifetime in CH3NH3PbBr3 Perovskite: Ab Initio Quantum Dynamics Simulation. *J. Phys. Chem. Lett.* **2020**, *11*, 9100−9109.
(38) Shi, R.; Fang, W. H.; Vasenko, A. S.; Long, R.; Prezhdo, O. V. Efficient Passivation of Dy Center in CH3NH3PbBr3 by Chlorine: Quantum Molecular Dynamics. *Nano Res.* **2022**, *15*, 2112−2122.
(39) Kresse, G.; Hafner, J. Ab Initio Molecular Dynamics for Liquid Metals. *Phys. Rev. B* **1993**, *47*, 558.
(40) Perdew, J. P.; Burke, K.; Ernzerhof, M. Generalized Gradient Approximation Made Simple. *Phys. Rev. Lett.* **1996**, *77*, 3865−3868.
(41) Kresse, G.; Joubert, D. From Ultrasoft Pseudopotentials to the Projector Augmented-Wave Method. *Phys. Rev. B* **1999**, *59*, 1758−1775.
(42) Momma, K.; Izumi, F. Vesta 3 for Three-Dimensional Visualization of Crystal, Volumetric and Morphology Data. *J. Appl. Crystallogr.* **2011**, *44*, 1272−1276.
(43) Zhang, L. F.; Han, J.; Wang, H.; Saidi, W. A.; Car, R.; Ee, W. In *End-to-End Symmetry Preserving Inter-Atomic Potential Energy Model for Finite and Extended Systems*; Adv Neural Inf Process Syst. 31; Bengio, S., Wallach, H., Larochelle, H., Grauman, K., Cesa-Bianchi, N., Garnett, R., Eds.; Curran Associates, Inc., 2018; pp 4441−4451.
(44) Andolina, C. M.; Williamson, P.; Saidi, W. A. Optimization and Validation of a Deep Learning Cuzr Atomistic Potential: Robust Applications for Crystalline and Amorphous Phases with near-Dft Accuracy. *J. Chem. Phys.* **2020**, *152*, 154701.
(45) Bayerl, D.; Andolina, C. M.; Dwaraknath, S.; Saidi, W. A. Convergence Acceleration in Machine Learning Potentials for Atomistic Simulations. *Digital Discovery* **2022**, *1*, 61−69.
(46) Saidi, W. A.; Choi, J. J. Nature of the Cubic to Tetragonal Phase Transition in Methylammonium Lead Iodide Perovskite. *J. Chem. Phys.* **2016**, *145*, 144702.
(47) Guo, Y.; Wang, Q.; Saidi, W. A. Structural Stabilities and Electronic Properties of High-Angle Grain Boundaries in Perovskite Cesium Lead Halides. *J. Phys. Chem. C* **2017**, *121*, 1715−1722.
(48) Shan, W.; Saidi, W. A. Segregation of Native Defects to the Grain Boundaries in Methylammonium Lead Iodide Perovskite. *J. Phys. Chem. Lett.* **2017**, *8*, 5935−5942.
(49) Saidi, W. A.; Poncé, S.; Monserrat, B. Temperature Dependence of the Energy Levels of Methylammonium Lead Iodide Perovskite from First-Principles. *J. Phys. Chem. Lett.* **2016**, *7*, 5247−5252.
(50) Saidi, W. A.; Kachmar, A. Effects of Electron−Phonon Coupling on Electronic Properties of Methylammonium Lead Iodide Perovskites. *J. Phys. Chem. Lett.* **2018**, *9*, 7090−7097.
(51) Meggiolaro, D.; Ambrosio, F.; Mosconi, E.; Mahata, A.; De Angelis, F. Polarons in Metal Halide Perovskites. *Adv. Energy Mater.* **2020**, *10* (15), 1902748.
(52) Miyata, K.; Meggiolaro, D.; Trinh, M. T.; Joshi, P. P.; Mosconi, E.; Jones, S. C.; De Angelis, F.; Zhu, X. Y. Large Polarons in Lead Halide Perovskites. *Sci. Adv.* **2017**, *3*, No. e1701217.
(53) Li, W.; Vasenko, A. S.; Tang, J. F.; Prezhdo, O. V. Anharmonicity Extends Carrier Lifetimes in Lead Halide Perovskites at Elevated Temperatures. *J. Phys. Chem. Lett.* **2019**, *10*, 6219−6226.
(54) Li, W.; Tang, J. F.; Casanova, D.; Prezhdo, O. V. Time-Domain Ab Lnitio Analysis Rationalizes the Unusual Temperature Dependence of Charge Carrier Relaxation in Lead Halide Perovskite. *ACS Energy Lett.* **2018**, *3*, 2713−2720.

https://doi.org/10.1021/acs.jpclett.2c01452
J. Phys. Chem. Lett. 2022, 13, 5946−5952

(55) Zhou, G. Q.; Chu, W. B.; Prezhdo, O. V. Structural Deformation Controls Charge Losses in MAPbI3: Unsupervised Machine Learning of Nonadiabatic Molecular Dynamics. *ACS Energy Lett.* **2020**, *5*, 1930−1938.
(56) Milot, R. L.; Eperon, G. E.; Snaith, H. J.; Johnston, M. B.; Herz, L. M. Temperature-Dependent Charge-Carrier Dynamics in CH3NH3PbI3 Perovskite Thin Films. *Adv. Funct. Mater.* **2015**, *25*, 6218−6227.
(57) Mangan, S. M.; Zhou, G. Q.; Chu, W. B.; Prezhdo, O. V. Dependence between Structural and Electronic Properties of CsPbI3: Unsupervised Machine Learning of Nonadiabatic Molecular Dynamics. *J. Phys. Chem. Lett.* **2021**, *12*, 8672−8678.
(58) Park, Y. S.; Guo, S. J.; Makarov, N. S.; Klimov, V. I. Room Temperature Single-Photon Emission from Individual Perovskite Quantum Dots. *ACS Nano* **2015**, *9*, 10386−10393.
(59) Aristidou, N.; Eames, C.; Sanchez-Molina, I.; Bu, X. N.; Kosco, J.; Islam, M. S.; Haque, S. A. Fast Oxygen Diffusion and Iodide Defects Mediate Oxygen-Induced Degradation of Perovskite Solar Cells. *Nat. Commun.* **2017**, *8*, 15218.
(60) He, J. L.; Fang, W. H.; Long, R.; Prezhdo, O. V. Superoxide/Peroxide Chemistry Extends Charge Carriers' Lifetime but Undermines Chemical Stability of CH3NH3PbI3 Exposed to Oxygen: Time-Domain Ab Initio Analysis. *J. Am. Chem. Soc.* **2019**, *141*, 5798−5807.
(61) Zhang, Z. S.; Fang, W. H.; Tokina, M. V.; Long, R.; Prezhdo, O. V. Rapid Decoherence Suppresses Charge Recombination in Multi-Layer 2d Halide Perovskites: Time-Domain Ab Initio Analysis. *Nano Lett.* **2018**, *18*, 2459−2466.
(62) Zhang, Z. S.; Fang, W. H.; Long, R.; Prezhdo, O. V. Exciton Dissociation and Suppressed Charge Recombination at 2d Perovskite Edges: Key Roles of Unsaturated Halide Bonds and Thermal Disorder. *J. Am. Chem. Soc.* **2019**, *141*, 15557−15566.
(63) Mahata, A.; Meggiolaro, D.; De Angelis, F. From Large to Small Polarons in Lead, Tin, and Mixed Lead-Tin Halide Perovskites. *J. Phys. Chem. Lett.* **2019**, *10*, 1790−1798.
(64) Neukirch, A. J.; Nie, W. Y.; Blancon, J. C.; Appavoo, K.; Tsai, H.; Sfeir, M. Y.; Katan, C.; Pedesseau, L.; Even, J.; Crochet, J. J.; et al. Polaron Stabilization by Cooperative Lattice Distortion and Cation Rotations in Hybrid Perovskite Materials. *Nano Lett.* **2016**, *16*, 3809−3816.
(65) Zhang, P. Z.; Hou, Z. F.; Jiang, L.; Yang, J.; Saidi, W. A.; Prezhdo, O. V.; Li, W. Weak Anharmonicity Rationalizes the Temperature-Driven Acceleration of Nonradiative Dynamics in Cu2znsns4 Photoabsorbers. *ACS Appl. Mater. Interfaces* **2021**, *13*, 61365−61373.
(66) Wu, Y. F.; Chu, W. B.; Vasenko, A. S.; Prezhdo, O. V. Common Defects Accelerate Charge Carrier Recombination in CsSnI3 without Creating Mid-Gap States. *J. Phys. Chem. Lett.* **2021**, *12*, 8699−8705.
(67) Kamisaka, H.; Kilina, S. V.; Yamashita, K.; Prezhdo, O. V. Ultrafast Vibrationally-Induced Dephasing of Electronic Excitations in PbSe Quantum Dot. *Nano Lett.* **2006**, *6*, 2295−2300.
(68) Long, R.; Prezhdo, O. V. Asymmetry in the Electron and Hole Transfer at a Polymer-Carbon Nanotube Heterojunction. *Nano Lett.* **2014**, *14*, 3335−3341.
(69) Wang, Z. L.; Altmann, P.; Gadermaier, C.; Yang, Y. T.; Li, W.; Ghirardini, L.; Trovatello, C.; Finazzi, M.; Duo, L.; Celebrano, M.; et al. Phonon-Mediated Interlayer Charge Separation and Recombination in a MoSe2/WSe2 Heterostructure. *Nano Lett.* **2021**, *21*, 2165−2173.
(70) Chu, W. B.; Saidi, W. A.; Prezhdo, O. V. Long-Lived Hot Electron in a Metallic Particle for Plasmonics and Catalysis: Ab Initio Nonadiabatic Molecular Dynamics with Machine Learning. *ACS Nano* **2020**, *14*, 10608−10615.
(71) Tomko, J. A.; Runnerstrom, E. L.; Wang, Y. S.; Chu, W. B.; Nolen, J. R.; Olson, D. H.; Kelley, K. P.; Cleri, A.; Nordlander, J.; Caldwell, J. D.; et al. Long-Lived Modulation of Plasmonic Absorption by Ballistic Thermal Injection. *Nat. Nanotechnol.* **2021**, *16*, 47−51.
(72) Xu, C.; Yong, H. W.; He, J. L.; Long, R.; Cadore, A. R.; Paradisanos, I.; Ott, A. K.; Soavi, G.; Tongay, S.; Cerullo, G.; et al. Weak Distance Dependence of Hot-Electron-Transfer Rates at the Interface between Monolayer MoS2 and Gold. *ACS Nano* **2021**, *15*, 819−828.
(73) Long, R.; English, N. J. Density Functional Theory Studies of Doping in Titania. *Mol. Simul.* **2010**, *36*, 618−632.
(74) Long, R.; English, N. J. Synergistic Effects on Band Gap-Narrowing in Titania by Codoping from First-Principles Calculations. *Chem. Mater.* **2010**, *22*, 1616−1623.
(75) Prezhdo, O. V. Modeling Non-Adiabatic Dynamics in Nanoscale and Condensed Matter Systems. *Acc. Chem. Res.* **2021**, *54*, 4239−4249.
(76) Zheng, Q. J.; Chu, W. B.; Zhao, C. Y.; Zhang, L. L.; Guo, H. L.; Wang, Y. N.; Jiang, X.; Zhao, J. Ab Initio Nonadiabatic Molecular Dynamics Investigations on the Excited Carriers in Condensed Matter Systems. *Wiley Interdiscip. Rev. Comput. Mol. Sci.* **2019**, *9*, No. e1411.
(77) Mai, S. B.; Gonzalez, L. Molecular Photochemistry: Recent Developments in Theory. *Angew. Chem., Int. Ed.* **2020**, *59*, 16832−16846.
(78) Smith, B.; Akimov, A. V. Modeling Nonadiabatic Dynamics in Condensed Matter Materials: Some Recent Advances and Applications. *J. Condens. Matter Phys.* **2020**, *32*, No. 073001.
(79) Wang, L. J.; Qiu, J.; Bai, X.; Xu, J. B. Surface Hopping Methods for Nonadiabatic Dynamics in Extended Systems. *Wiley Interdiscip. Rev. Comput. Mol. Sci.* **2020**, *10*, No. e1435.
(80) Jankowska, J.; Sobolewski, A. L. Modern Theoretical Approaches to Modeling the Excited-State Intramolecular Proton Transfer: An Overview. *Mol.* **2021**, *26*, 5140.
(81) Richings, G. W.; Habershon, S. Predicting Molecular Photochemistry Using Machine-Learning-Enhanced Quantum Dynamics Simulations. *Acc. Chem. Res.* **2022**, *55*, 209−220.

https://doi.org/10.1021/acs.jpclett.2c01452
J. Phys. Chem. Lett. 2022, 13, 5946−5952